A device library for the ultra-low loss Si3N4 platform

Q Wilmart, S Guerber, J Faugier-Tovar, Yasmine Ibrahimi, Camille Petit-Etienne, Laurene Youssef, Carole Socquet-Clerc, André Myko, Karen Ribaud, François Duport, et al.

A device library for the ultra-low loss Si_3N_4 platform

Q. Wilmart[a], S. Guerber[a], J. Faugier-Tovar[a], Yasmine Ibrahimi[b], Camille Petit-Etienne[c], Laurene Youssef[c], Carole Socquet-Clerc[a], André Myko[a], Karen Ribaud[a], François Duport[b], Erwine Pargon[c], Frédéric Van Dijk[c]

[a]Université Grenoble Alpes, CEA, LETI, MINATEC Campus, CEA-Grenoble, Grenoble, France; [b]Thales Research and Technology France, 84360 Palaiseau, Ile de France, France, III-V Lab, Palaiseau, Ile de France, France; [c]Université Grenoble Alpes, CNRS, CEA/LETI-Minatec, Grenoble INP, LTM, F-38054, Grenoble, France

ABSTRACT

Silicon nitride platforms based on ultra-low loss tightly confining waveguides present a great interest for a wide range of applications. We present our 200mm platform based on 800nm-thick LPCVD Si_3N_4 with optical losses below 5dB/m. It is completed with a set of photonic components specially developed for this platform: grating and edge fiber couplers, directional couplers, MMI, Y-junction, racetrack resonators and an AWG multiplexer. The Si_3N_4 platform and its device library are the basic building blocks for more complex circuits targeting advanced applications: LiDAR, microwave optics, quantum photonics, neuromorphic computing and sensors.

Keywords: Si_3N_4, Photonics, Waveguide, Resonator, Grating Coupler

1. INTRODUCTION

The last few years have shown the success of silicon nitride platforms for ultra-low loss tightly confining waveguides [1]–[6]. These platforms are ideal for nonlinear photonics, thanks to the high Kerr nonlinearity, the high power handling capability the small bending radii and of course the low propagation losses of Si_3N_4 waveguides. Therefore, the potential for applications is huge: LiDAR, microwave optics, quantum photonics, neuromorphic computing, telecommunication, sensors… As silicon nitride photonic circuit being based on CMOS technology, it is easily accessible to foundries for low-cost and mass production. The integrated nature of this solution opens the way to high performance, compact and energy efficient applications of nonlinear optics such as for example massively parallel data communications [7]–[9] and quantum computing [10]. Recent studies report propagation losses on the order of the dB/m and quality factor of ring resonators up to tens of millions in high confinement, multimode waveguides (see for example table I of [5]). The race for ultra-low propagation losses and high quality factors has driven fabrication platforms towards wide multimode waveguides. However, in many applications, designers will need routing components capable to operate in the single mode regime or with a tight bending radius. The main fabrication challenges (mainly due to the high stress of a thick stoichiometric Si_3N_4 layer) have been addressed and the next step is to increase the maturity of component and circuit designs. Following the successful example of silicon photonics, few Si_3N_4 platforms are now available through Multi Project Wafers run [11], [12]. As for silicon photonics, a Process Design Kit (PDK) including a device library is then expected.

In this article, we present our 200mm platform based on high confinement 800nm-thick Si_3N_4 waveguides featuring very low optical losses down to 3dB/m. The high confinement enables compact circuits thanks to tight waveguide bends, down to 20µm radius. In order to ease the design of photonic circuits we developed a library for basic routing and coupling components (1x2 and 2x2 MMI, directional couplers, Y-junction, grating coupler) for which we provide detailed measurements. In addition, we show two examples of more advanced devices: an Arrayed Waveguide Grating (AWG) multiplexer and a Distributed Bragg Reflector (DBR) for hybrid Si_3N_4/III-V laser.

2. FABRICATION DATA

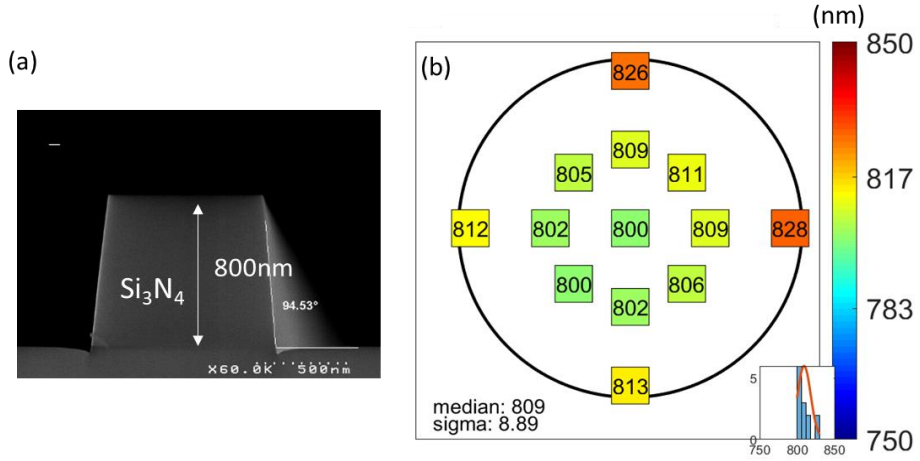

Figure 1: (a) SEM cross section of the single mode waveguide. (b) Wafer mapping of Si_3N_4 thickness.

The fabrication starts with a 200mm silicon substrate, which is oxidized over 3µm. The deposition of the 800nm-thick, high-strain film of stoichiometric Si_3N_4 is done using Low Pressure Chemical Vapor Deposition (LPCVD) at 780°C. The process is performed following the twist-and-grow method [2], [13]: a two-steps deposition of 400nm Si_3N_4 with wafer rotation of 45° is apply to avoid possible cracks and film delamination due to the high tensile strain. An ellipsometry measurement of the film thickness is shown in Figure 1b. The Si_3N_4 film on the backside is removed in a subsequent step. The film is then patterned using 248nm Deep Ultra-Violet photolithography and dry etching (see cross section in Figure 1a). The presence of "dummy" structures ensures a good uniformity of the etching as well as a good reproducibility of the etching step when the mask is changed. Fields are photorepeated over the wafer with a die size of 22x22mm^2. Then, the wafer undergoes a series of thermal annealing in O_2, H_2 and N_2 atmospheres (see [2]). The waveguides are then encapsulated using High Density Plasma (HDP) oxide deposition. The process includes a deep

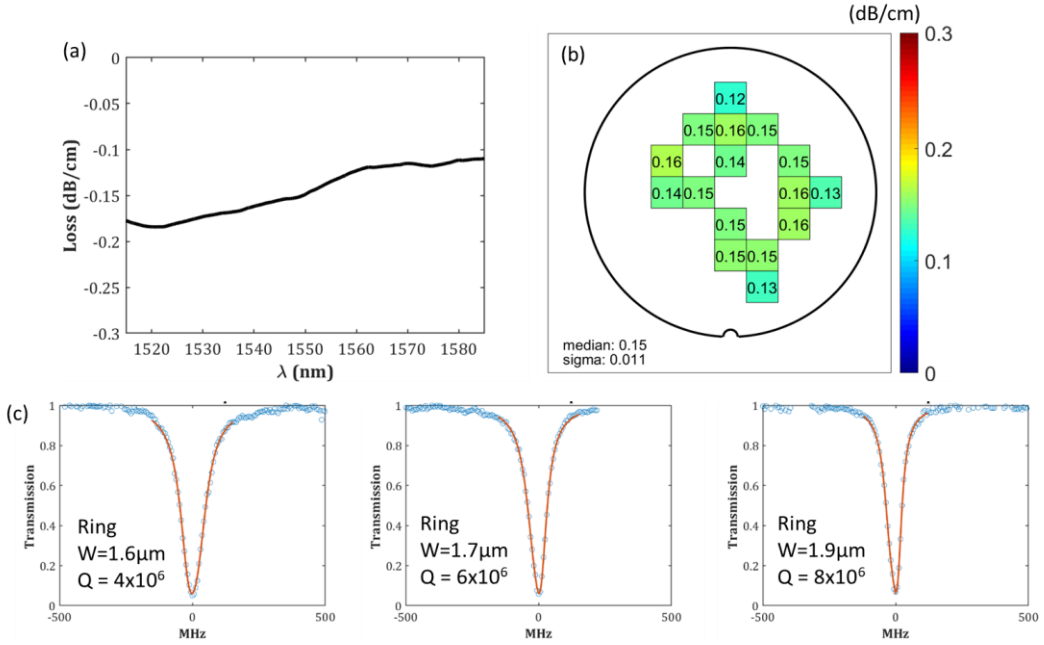

Figure 2: (a) Propagation loss spectrum of the single mode waveguide extracted from the cut back measurement. (b) Mapping of single mode waveguide propagation losses at 1550nm (in dB/cm). (c) 112µm-radius ring resonator spectra with waveguide width of 1.6, 1.7 and 1.9µm (from left to right respectively). An intrinsic quality factor Q of 4, 6 and 8 million respectively is extracted.

etching of large trenches through the oxide and the silicon substrate enabling a substrate clearing and an optical quality facet for edge fiber coupling.

3. PROPAGATION LOSS MEASUREMENT

The first criteria to evaluate the Si_3N_4 waveguide performance is the optical propagation loss. We use two types of structures to evaluate the losses: spiraled delay lines of various lengths based on single-mode waveguides and ring resonators based on slightly multimode waveguides. The single mode waveguide is 900nm-wide. We consider delay lines of lengths 20, 40 and 60cm. The cut-back method allows us to extract the loss spectrum averaged over 16 measurements in different locations of the wafer as shown in Figure 2a. We show as well the wafer mapping of the propagation losses at 1550nm in Figure 2b. They are mainly uniform on the 200mm wafer with a range of 0.12-0.16dB/cm.

The ring resonator method is more adapted to the measurement of very low losses, which are expected in larger waveguides. Considering losses of a few dB/m, meters long delay lines would be required for an accurate measurement. Here, we consider ring resonators of 112µm radius based on 1.6, 1.7 and 1.9µm wide waveguide for which 2 to 3 TE modes can be supported. The test cell includes structures with different ring-bus distances (referred as gap in the following) in order to identify the critical coupling geometry. The measurement is performed using a tunable laser (resolution of 0.05pm) and its associated photodetector. Resonance measurements with their Lorentzian fit of resonators at critical coupling with 1.6, 1.7 and 1.9µm-wide waveguides are shown in Figure 2c. We extract intrinsic Q-factors of 4, 6 and 8 million respectively, corresponding to ~6, 5 and 3 dB/m propagation losses. At the largest gap value (600nm) the resonator operates in the under-coupling regime. In this case, we observe a resonance splitting which is generally attributed to the backscattering occurring in very high quality factor rings [2], [14].

The loss measurement is comparable to previously reported values while being lower than some reports [1] with wider waveguides but we observe a decreased in losses when increasing the width.

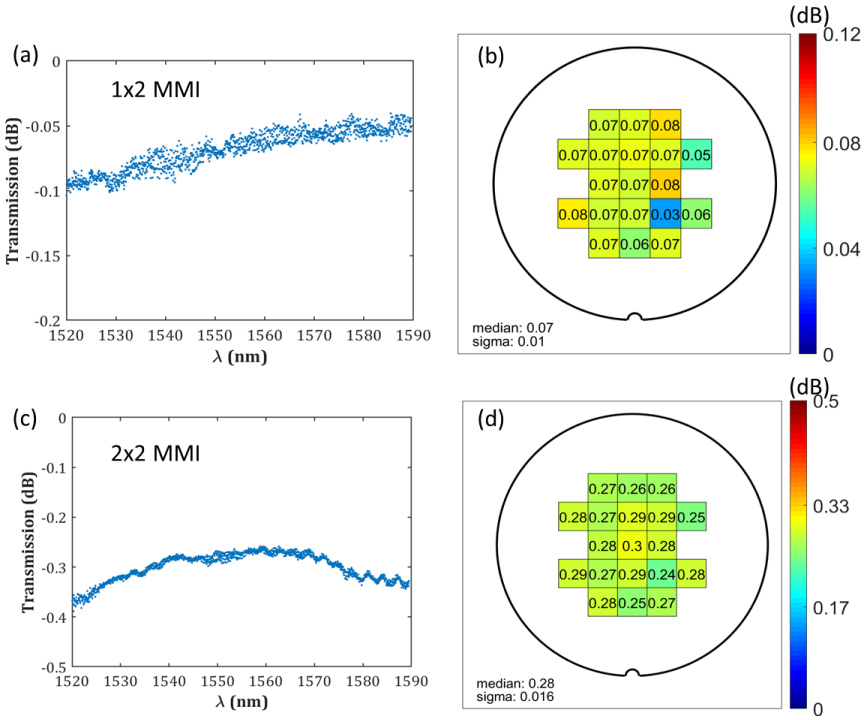

Figure 3: MMI measurement. (a) 1x2 MMI spectrum. (b) 1x2 MMI wafer map insertion losses (in dB). (c) and (d) same as (a) and (b) but for the 2x2 MMI.

4. DEVICE LIBRARY

4.1 Routing components

Designers and end users of photonic circuits need to rely on mature and stable fabrication platforms, supported by a PDK and a reliable device library. In the following, we present basic routing and coupling components fabricated on the low-loss Si_3N_4 platform.

- Bend waveguide

Bend waveguide are of course an essential component. Designers need to know the minimum bend radius one can use and the associated losses. We measure the transmission of series of 50 circular bends of 10, 20, 40 and 60µm radiuses. Only the 10µm radius bend shows higher losses. Radiuses of 20µm and above show constant losses <0.01dB/90°. As a result, a 20µm-radius bend can be used safely for single mode waveguides. This result emphasizes the very good compactness of the high confinement Si_3N_4 platform.

- Multimode Interferometer (MMI)

MMIs are useful to combine or split optical signals with a reliable 50% coupling ratio. Therefore, we used a Design of Experiment (DOE) based on geometrical parameters, to determine the nominal MMI for the photonic library, i.e. the one with the lowest insertion losses. Results are shown in Figure 3. The nominal 1X2 MMI has a length of 13µm and features insertion losses of 0.07dB with a good wafer uniformity (range 0.05-0.08dB). The nominal 2X2 MMI has a length of 40.5µm and shows losses of 0.28dB (range 0.24-0.30dB).

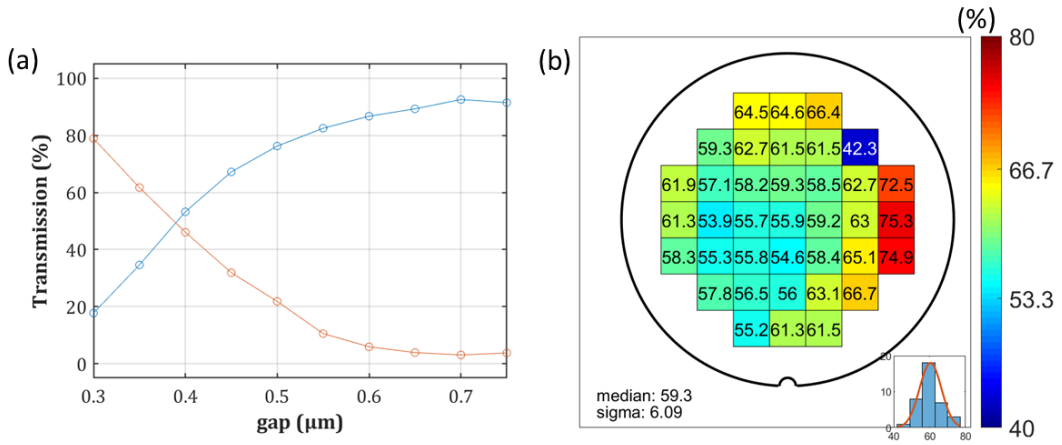

Figure 4: Directional coupler measurement. (a) Coupling ratio of the 2 outputs of the DC as a function of the waveguide distance (gap). (b) Wafer map of the coupling ratio for the 400nm gap.

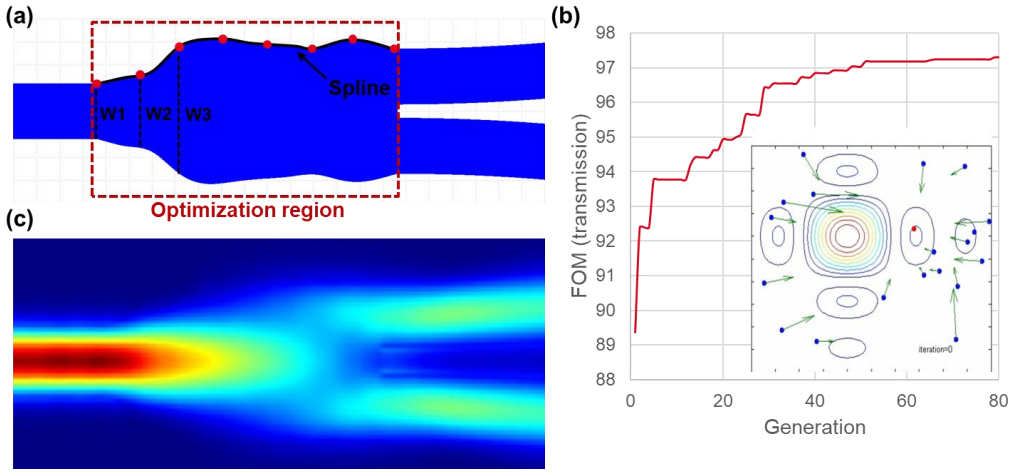

Figure 5: (a) Top view of the Y junction with the optimization region. (the blue shape is the actual Y junction layout). (b) Evolution of the FOM during the optimization (16 particles). (c) 2DFDTD Simulation of the power over the optimized Y junction.

- Directional coupler (DC)

Compared to MMIs, the coupling ratio of a DC is less reliable but it can be easily tuned by varying the waveguide gap. Figure 4a shows the coupling ratio as a function of the waveguide gap of a 20µm long DC. The coupling ratio is particularly sensitive to geometrical parameters (Si_3N_4 thickness and waveguide width). As a result, its variation over the wafer is significant as shown in the mapping of Figure 4a. However, by selecting the central dies the range of coupling ration for a given DC is <8%. Finally, we evaluate the insertion loss of the DC by measuring the transmission of 50 DC in series: we obtain 0.1dB insertion loss.

- Y junction

The Y junction is more simple and compact than other power splitters. Its intrinsic symmetry helps to guarantee a low power imbalance between the output waveguides. However, this structure usually suffers from high insertion losses (>1dB) due to the sharp gap in the middle of the output waveguides. Those high losses could be mitigated by optimizing the Y junction core shape [15]. Using this principle, we have designed a low loss Y junction. As shown on Figure 5a, the middle region of the Y junction is divided into segments (10 in our case) for which the width defines a spline curve. The optimization region length is 6.5µm. The width of each segment is found using a Particle Swarm Optimization (PSO). As shown on Figure 5b, the algorithm maximizes a Figure of Merit (FOM) which is the total transmission of the device (sum of the two-output waveguides power) computed in a 2DFDTD simulation. As shown in Figure 5b, after 80 generation, a transmission higher than 97% is obtained.

We perform a measurement of 50 Y-junction in series to extract the losses. This measurement is repeated over 19 dies of a wafer. We obtain a median value of insertion losses of 0.12dB and a standard deviation of 0.025dB.

A summary of power splitter devices performances is shown in Table 1. We indicate the median insertion loss and its standard deviation (measured over 19 dies of a wafer). In conclusion, when one needs an optical splitter, MMI is preferred for a reliable and low loss splitting of 50%. The Y-junction can be used when high compactness is needed at the expense of slightly higher losses. The DC is a low-loss, tunable alternative but the exact splitting ratio is less reliable.

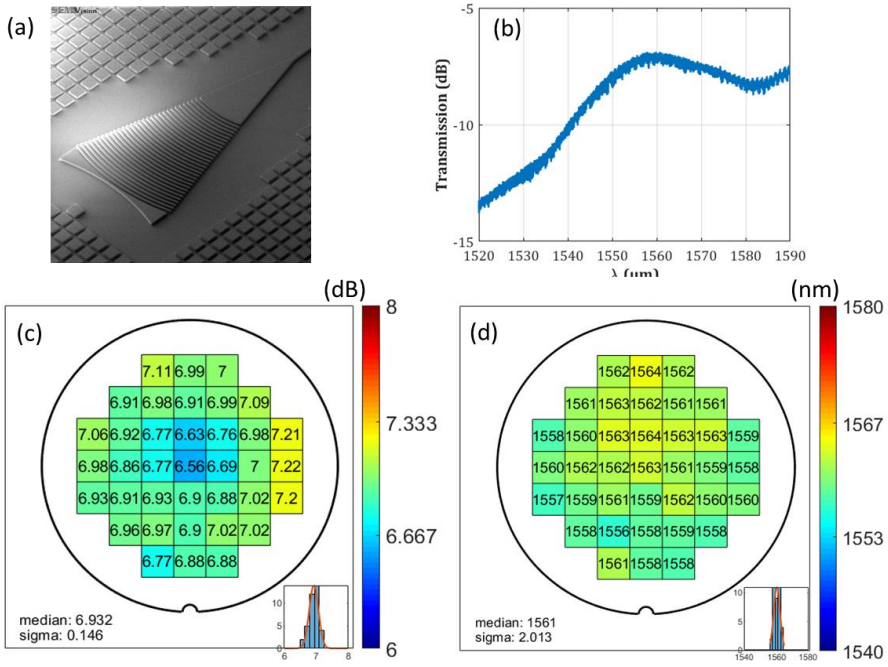

Figure 6: Grating coupler measurement. (a) SEM image of the grating fiber coupler. (b) Transmission spectrum. (c) Wafer map of insertion losses. (d) Wafer map of central wavelength

Table 1. Performances of power splitter devices

Device	**1x2 MMI**	**2x2 MMI**	**DC**	**Y-junction**
Insertion loss (dB)	0.07	0.28	0.1	0.12
Standard deviation (dB)	0.01	0.02	0.01	0.025

4.2 Coupling components

- Grating fiber coupler

Grating fiber couplers enable reproducible and easy optical characterizations. Even if they are generally not used in packaged circuits due to their relatively high losses and limited bandwidth, they are particularly useful for rapid, wafer-level test of components. We developed a grating fiber coupler for Single Mode Fiber (SMF) top coupling at an angle of 11.5° (8° in SiO2). It is based on the full etching of the 800nm-thick Si_3N_4 layer with a focusing function to limit the length of the grating-to-waveguide taper (see Figure 6a). The transmission spectrum of the grating coupler is shown in Figure 6b. The mappings of the central wavelength and the insertion loss at the central wavelength are shown in Figure 6c and d respectively. The median value of insertion losses of 6.9dB is higher than one would expect from an edge coupler but it is very uniform over the wafer with a standard deviation of 0.15dB. As well, the central wavelength shows a good reproducibility over the wafer. Note that all the routing components presented in the previous section are characterized using this grating as a fiber coupler.

4.3 Arrayed Waveguide Grating (AWG) multiplexer

Among the various architectures of multiplexer and demultiplexer, the AWG is probably the most versatile. Indeed, a wide range of channel spacing can be achieved by changing the dimensions of the waveguide array that defines the spectral dispersion of the AWG. With careful optimization and proper fabrication, low insertion losses as well as a low crosstalk level can be obtained [16]. As a proof of concept, we have design and characterize a C-band, 8 channels AWG on our SiN platform (see SEM image in Figure 7a). The channel spacing is 300GHz, the array order is 32 and the device footprint is 1700 * 800 μm^2. The measured transmission of the device is shown in Figure 7b. The insertion losses are below 3.5dB, the crosstalk is lower than 15dB. The channel spacing is close to the designed one (300GHz). A spectral shift of ~2nm has been observed between the channels central wavelength and the original design grid, it is attributed to fabrication variations.

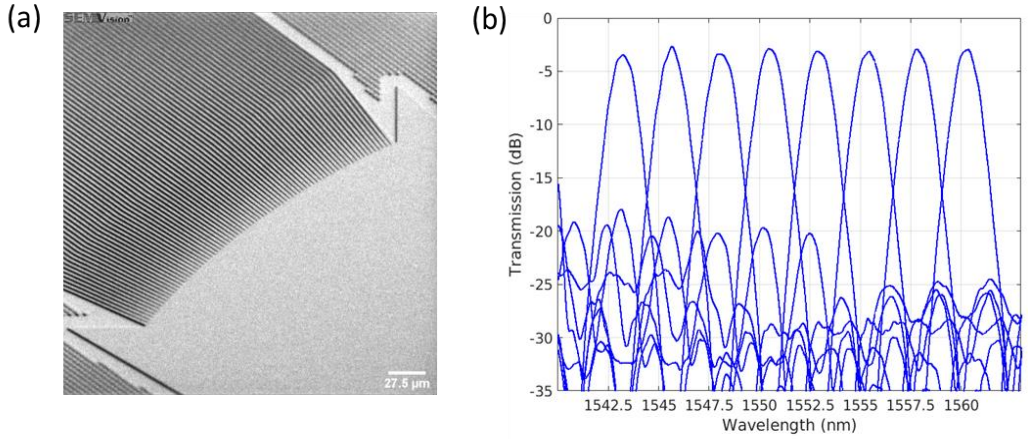

Figure 7: (a) SEM view of the AWG multiplexer. (b) AWG transmission measurement.

4.4 Distributed Bragg Reflector (DBR)

We have developed a DBR laser using a hybrid design that consists of two chips: an RSOA (Reflective Semiconductor Amplifier) and a passive Si_3N_4 chip. The RSOA is developed at III-VLab using a SIBH (Semi-Insulating Buried Heterostructure) structure [17]. It provides a 20 dB gain centred around 1550 nm to compensate for the losses in the passive part of the laser. The RSOA has an output waveguide tilted by 7° to minimize the effect of back reflections at the interface between the two chips (Figure 8a).
The passive Si_3N_4 chip originates from a wafer fabricated in parallel to the one described in the previous sections. For a DBR laser, the passive circuits contain two elements: the 6 mm long Bragg grating and the interface with the RSOA containing an optical mode adapter tilted by 15° at the interface to match the angle of the RSOA optical port.
The Bragg grating must have a bandwidth narrow enough to yield a single-mode operation. To this end, we chose a 5th order Bragg grating. The gap and posts height are designed to get the proper grating coupling strength according to the desired refractive effective index variation. We use a dynamic alignment set up to butt-couple the two chips. We measured the optical spectrum (Figure 8b) using a high-resolution OSA (optical spectrum analyser), which shows an SMSR of 55 dB, and an FSR (Free Spectral Range) of 15.21 GHz. These performances are comparable with previous results obtained using butt coupling between an RSOA and low-confinement Si_3N_4 passive chip developed also at the CEA Leti [18] which allow us to validate the high confinement platform featuring a much higher compacity and prepare for more complex designs.

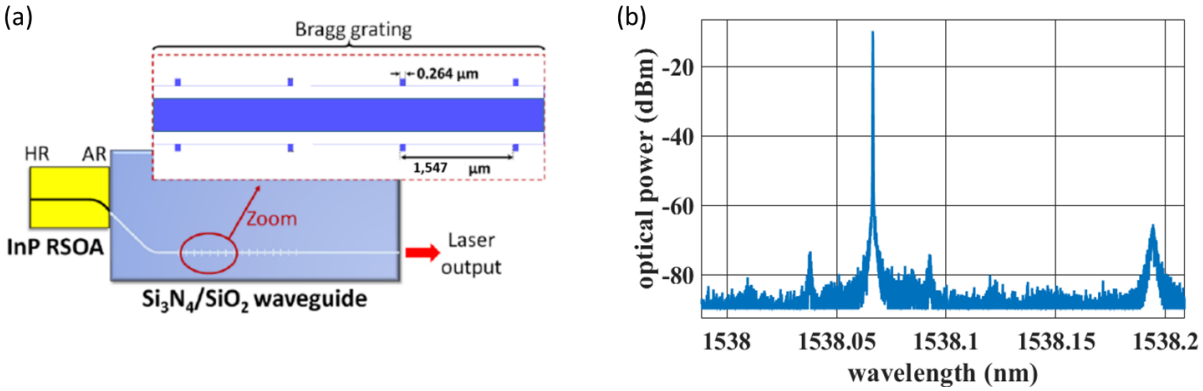

Figure 8: (a) The DBR laser components: RSOA and Si_3N_4 chip. The zoom shows the dimensions of the Bragg grating. (b) The optical spectrum of the DBR laser showing a 55 dB SMSR and 15.21 GHz FSR

5. CONCLUSION

Following several demonstrations of ultra-low loss Si_3N_4 waveguides by various groups, in this paper we make a step towards the platform maturity by showing a library of passive photonic components. In addition to ultra-low propagation losses of a few dB/m, we presented experimental performances of grating coupler, MMI, directional couplers, Y-junction, AWG multiplexer and DBR. These devices will feed a tool box for circuit designers targeting advanced applications such as quantum computing and communication, microwave optics, neuromorphic computing and telecommunication.

ACKNOWLEDGEMENT

This research was supported by the French RENATECH network.

REFERENCES

[1] J. Liu *et al.*, « High-yield, wafer-scale fabrication of ultralow-loss, dispersion-engineered silicon nitride photonic circuits », *Nat. Commun.*, vol. 12, nº 1, p. 2236, déc. 2021, doi: 10.1038/s41467-021-21973-z.

[2] H. El Dirani *et al.*, « Ultralow-loss tightly confining Si_3N_4 waveguides and high-Q microresonators », *Opt. Express*, vol. 27, nº 21, p. 30726, oct. 2019, doi: 10.1364/OE.27.030726.

[3] M. H. P. Pfeiffer *et al.*, « Photonic Damascene Process for Low-Loss, High-Confinement Silicon Nitride Waveguides », *IEEE J. Sel. Top. Quantum Electron.*, vol. 24, nº 4, p. 1-11, juill. 2018, doi: 10.1109/JSTQE.2018.2808258.

[4] Y. Xuan *et al.*, « High-Q silicon nitride microresonators exhibiting low-power frequency comb initiation », *Optica*, vol. 3, nº 11, p. 1171, nov. 2016, doi: 10.1364/OPTICA.3.001171.

[5] X. Ji, S. Roberts, M. Corato-Zanarella, et M. Lipson, « Methods to achieve ultra-high quality factor silicon nitride resonators », *APL Photonics*, vol. 6, nº 7, p. 071101, juill. 2021, doi: 10.1063/5.0057881.

[6] Z. Ye, K. Twayana, P. A. Andrekson, et V. Torres-Company, « High-Q Si_3N_4 microresonators based on a subtractive processing for Kerr nonlinear optics », *Opt. Express*, vol. 27, nº 24, p. 35719, nov. 2019, doi: 10.1364/OE.27.035719.

[7] A. L. Gaeta, M. Lipson, et T. J. Kippenberg, « Photonic-chip-based frequency combs », *Nat. Photonics*, vol. 13, nº 3, p. 158-169, mars 2019, doi: 10.1038/s41566-019-0358-x.

[8] B. Stern, X. Ji, Y. Okawachi, A. L. Gaeta, et M. Lipson, « Battery-operated integrated frequency comb generator », *Nature*, vol. 562, nº 7727, p. 401-405, oct. 2018, doi: 10.1038/s41586-018-0598-9.

[9] P. Marin-Palomo *et al.*, « Microresonator-based solitons for massively parallel coherent optical communications », *Nature*, vol. 546, nº 7657, p. 274-279, juin 2017, doi: 10.1038/nature22387.

[10] V. D. Vaidya *et al.*, « Broadband quadrature-squeezed vacuum and nonclassical photon number correlations from a nanophotonic device », *Sci. Adv.*, vol. 6, nº 39, p. eaba9186, sept. 2020, doi: 10.1126/sciadv.aba9186.

[11] « https://mycmp.fr/Si3N4-800/ ».

[12] « https://www.ligentec.com/ligentec-foundry/mpw/ ».

[13] H. El Dirani *et al.*, « Crack-Free Silicon-Nitride-on-Insulator Nonlinear Circuits for Continuum Generation in the C-Band », *IEEE Photonics Technol. Lett.*, vol. 30, nº 4, p. 355-358, févr. 2018, doi: 10.1109/LPT.2018.2790045.

[14] K. Wu et A. W. Poon, « Stress-released Si_3N_4 fabrication process for dispersion-engineered integrated silicon photonics », *Opt. Express*, vol. 28, nº 12, p. 17708, juin 2020, doi: 10.1364/OE.390171.

[15] Y. Zhang *et al.*, « A compact and low loss Y-junction for submicron silicon waveguide », *Opt. Express*, vol. 21, nº 1, p. 1310, janv. 2013, doi: 10.1364/OE.21.001310.

[16] S. Pathak, D. Van Thourhout, et W. Bogaerts, « Design trade-offs for silicon-on-insulator-based AWGs for (de)multiplexer applications », *Opt. Lett.*, vol. 38, nº 16, p. 2961, août 2013, doi: 10.1364/OL.38.002961.

[17] Boust et al., « Single-mode and multi-mode DBR lasers using InP-Si3N4/SiO2 integration », *In : ECIO2020, European Conference on Integrated Optics (ECIO). 2020. p. S7.*, 2020.

[18] F. Duport *et al.*, « Directly modulated high power semiconductor optical amplifier », in *2018 International Topical Meeting on Microwave Photonics (MWP)*, Toulouse, oct. 2018, p. 1-4. doi: 10.1109/MWP.2018.8552859.